Astronomy & Astrophysics

Optical validation and characterization of *Planck* PSZ1 sources at the Canary Islands observatories

I. First year of ITP13 observations

R. Barrena[1,2], A. Streblyanska[1,2], A. Ferragamo[1,2], J. A. Rubiño-Martín[1,2], A. Aguado-Barahona[1,2],
D. Tramonte[1,2,3], R. T. Génova-Santos[1,2], A. Hempel[4], H. Lietzen[5], N. Aghanim[6], M. Arnaud[7,8], H. Böhringer[9],
G. Chon[9], J. Democles[7,8], H. Dahle[10], M. Douspis[6], A. N. Lasenby[11,12], P. Mazzotta[13], J. B. Melin[7,8],
E. Pointecouteau[14,15], G. W. Pratt[7,8], M. Rossetti[16], and R. F. J. van der Burg[7,8,17]

[1] Instituto de Astrofísica de Canarias, C/ Vía Láctea s/n, 38205 La Laguna, Tenerife, Spain
  e-mail: rbarrena@iac.es
[2] Universidad de La Laguna, Departamento de Astrofísica, 38206 La Laguna, Tenerife, Spain
[3] University of KwaZulu-Natal, Westville Campus, Private Bag X54001, Durban 4000, South Africa
[4] Universidad Andrés Bello, Departamento de Ciencias Físicas, 7591538 Santiago de Chile, Chile
[5] Tartu Observatory, University of Tartu, 61602 Tõravere, Tartumaa, Estonia
[6] Institut d'Astrophysique Spatiale, Université Paris-Sud, CNRS, UMR8617, 91405 Orsay Cedex, France
[7] IRFU, CEA, Université Paris-Saclay, 91191 Gif-sur-Yvette, France
[8] Université Paris Diderot, AIM, Sorbonne Paris Cité, CEA, CNRS, 91191 Gif-sur-Yvette, France
[9] Max-Planck-Institut für Extraterrestrische Physik, 85748 Garching, Germany
[10] Institute of Theoretical Astrophysics, University of Oslo, PO Box 1029, Blindern, 0315 Oslo, Norway
[11] Astrophysics Group, Cavendish Laboratory, JJ Thomson Av., Cambridge 3 ΘHE, UK
[12] Kavli Institute for Cosmology, Madingley Road, Cambridge 3 ΘHA, UK
[13] Dipartimento di Fisica, Università degli Studi di Roma "Tor Vergata", Via della Ricerca Scientifica 1, 00133 Roma, Italy
[14] Université de Toulouse, UPS-OMP, Institut de Recherche en Astrophysique et Planétologie (IRAP), 31400 Toulouse, France
[15] CNRS, IRAP, 9 avenue Colonel Roche, BP 44346, 31028 Toulouse Cedex 4, France
[16] IASF-Milano, Istituto Nazionale di Astrofisica, Via Bassini 15, 20133 Milano, Italy
[17] European Southern Observatory, Karl-Schwarzschild-Str. 2, 85748 Garching, Germany

ABSTRACT

We have identified new clusters and characterized previously unknown *Planck* Sunyaev–Zeldovich (SZ) sources from the first *Planck* catalogue of SZ sources (PSZ1). The results presented here correspond to an optical follow-up observational programme developed during approximately one year (2014) at Roque de los Muchachos Observatory, using the 2.5 m *Isaac Newton* telescope, the 3.5 m Telescopio Nazionale *Galileo*, the 4.2 m *William Herschel* telescope and the 10.4 m Gran Telescopio Canarias. We have characterized 115 new PSZ1 sources using deep optical imaging and spectroscopy. We adopted robust criteria in order to consolidate the SZ counterparts by analysing the optical richness, the 2D galaxy distribution, and velocity dispersions of clusters. Confirmed counterparts are considered to be validated if they are rich structures, well aligned with the *Planck* PSZ1 coordinate and show relatively high velocity dispersion. Following this classification, we confirm 53 clusters, which means that 46% of this PSZ1 subsample has been validated and characterized with this technique. Sixty-two SZ sources (54% of this PSZ1 subset) remain unconfirmed. In addition, we find that the fraction of unconfirmed clusters close to the galactic plane (at $|b| < 25°$) is greater than that at higher galactic latitudes ($|b| > 25°$), which indicates contamination produced by radio emission of galactic dust and gas clouds on these SZ detections. In fact, in the majority of the cases, we detect important galactic cirrus in the optical images, mainly in the SZ target located at low galactic latitudes, which supports this hypothesis.

Key words. large-scale structure of Universe – galaxies: clusters: general – catalogs

1. Introduction

The Sunyaev–Zeldovich (SZ) effect (Sunyaev & Zeldovich 1972) is a spectral distortion of the cosmic microwave background (CMB) generated by high energy electrons interacting with hot CMB photons through inverse Compton scattering. The SZ effect has in recent years become a powerful tool in cosmology that can complement the information obtained from the CMB angular power spectrum (e.g. Birkinshaw 1999;

Carlstrom et al. 2002; Planck Collaboration XX 2014; Planck Collaboration XXI 2014; Planck Collaboration XXIX 2014). Nowadays, one of the most common applications of the SZ effect is the detection of galaxy clusters. These gravitationally bound systems emerge as massive structures in the cosmic web of the large-scale structure (e.g. Springel et al. 2005). Galaxy clusters encompass several components, including dark and baryonic matter (e.g. Allen et al. 2011). For this reason, galaxy clusters are excellent laboratories for testing cosmology

and establishing constraints on cosmological parameters such as dark matter, dark energy densities, and the equation of state of the dark energy and neutrino masses (Vikhlinin et al. 2009; Henry et al. 2009; Mantz et al. 2010; Planck Collaboration XX 2014; Mantz et al. 2015; Planck Collaboration XXIV 2016).

The SZ effect is particularly evident when CMB photons interact, following the inverse Compton mechanism, with massive haloes that have a high content of hot gas. The net effect on the initial Planck spectrum of the CMB is to shift it to higher frequencies. While the surface brightness of the SZ effect is independent of redshift, cluster counts at high redshift are very sensitive to the cosmology (see e.g. Borgani & Guzzo 2001). Nevertheless, these massive structures are predicted to be very scarce in the ΛCDM model, and their abundance strongly decreases at high redshift (e.g. Springel et al. 2005). Therefore, the detection of galaxy clusters via the SZ effect, now accessible also with all-sky surveys, can be used for surveying large volumes and for constraining cosmological parameters.

In recent decades, all-sky surveys have been conducted using either optical or X-ray observations. Examples of optical surveys include catalogues based on SDSS data (Koester et al. 2007; Wen et al. 2009, 2012; Hao et al. 2010; Szabo et al. 2011), which are complete up to $z \sim 0.3$ for galaxies with magnitudes $M_r < -22$, reaching a limit of about $z \sim 0.5$. Examples of X-ray surveys are the ROSAT All-Sky Survey (RASS) and their corresponding catalogues (e.g. REFLEX, Böhringer et al. 2001, 2014; MACS, Ebeling et al. 2001; and NORAS, Böhringer et al. 2000), which extend to similar redshifts. Concerning millimetre surveys, in the last few years, remarkable efforts have yielded the first complete lists of galaxy clusters compiled through the thermal SZ effect, such as the surveys carried out with the Atacama Cosmology Telescope (ACT; Marriage et al. 2011; Hasselfield et al. 2013) and the South Pole Telescope (SPT; Staniszewski 2009; Vanderlinde et al. 2010; Williamson et al. 2011; Reichardt et al. 2013; Bleem et al. 2015).

The *Planck*[1] satellite (Planck Collaboration I 2014) provided the first opportunity to detect galaxy clusters through the SZ effect in a full sky survey (Planck Collaboration VIII 2011; Planck Collaboration XXIX 2014; Planck Collaboration XXVII 2016). Nevertheless, some SZ detections may correspond to misidentifications (in particular those with low SZ signal) or contamination due to the galactic dust contribution. In addition, the SZ effect provides no information about the redshift of the clusters. For all these reasons, dedicated follow-up programmes are important to make the resulting catalogues scientifically useful. In 2010, the *Planck* collaboration started intensive follow-up programmes to confirm SZ cluster candidates, first from intermediate versions of the *Planck* SZ catalogue (Planck Collaboration IX 2011; Planck Collaboration Int. I 2012; Planck Collaboration Int. IV 2013), second from the first public SZ catalogue (PSZ1; Planck Collaboration XXIX 2014; Planck Collaboration XXXII 2015), and finally from the second public SZ catalogue (PSZ2; Planck Collaboration XXVII 2016). Examples of optical follow-up of unknown SZ candidates are the observational programme performed with the RTT150 telescope (Planck Collaboration Int. XXVI 2015), that carried out at the Canary Islands observatories (Planck Collaboration

Int. XXXVI 2016), and the validation based on MegaCam at the 3.6 m Canadian France Hawaii Telescope (van der Burg et al. 2016; hereafter vdB+16). The RTT150 programme confirmed 79 PSZ1 clusters (47 of which were previously unknown), thereby determining photometric and spectroscopic redshift in the range $0.08 < z < 0.83$. This technique is also followed by Planck Collaboration Int. XXXVI (2016), confirming 73 PSZ1 clusters and providing their redshifts (in the range $0.09 < z < 0.82$). They also report no counterparts found for five additional cases. Finally, van der Burg et al. (2016) investigated a sample of 28 PSZ1 and PSZ2 candidates that were pre-selected using WISE and SDSS as high redshift ($z > 0.5$) candidates, with deep r- and z-band imaging from MegaCam/CFHT.

In this paper, we have continued the optical characterization of PSZ1 SZ sources started in Planck Collaboration Int. XXXVI (2016). The main motivation for these studies is to validate and identify cluster counterparts of unknown PSZ1 sources.

The paper is organized as follows. In Sect. 2, we describe the *Planck* PSZ1 catalogue and detail the observational follow-up. In Sect. 3, we describe the technique used to identify and confirm the cluster counterparts. Sect. 4 includes a detailed description of the nature of some relevant SZ targets (multiple detections, presence of gravitational arcs, fossil systems, etc.). Finally, in Sect. 5 we present the conclusions.

2. PSZ1 and optical follow-up observations

2.1. The PSZ1 as reference catalogue

Our reference cluster sample is PSZ1 (Planck Collaboration XXIX 2014; Planck Collaboration XXXII 2015). This catalogue includes 1227 clusters and cluster candidates derived from SZ effect detections using all-sky maps produced within the first 15.5 months of *Planck* observations. Briefly, SZ sources are selected using three different detection methods: MMF1, MMF3, and PwS. All sources included in the PSZ1 catalogue were detected by at least one of these three detection methods with a signal-to-noise ratio (S/N) of 4.5 or higher. Planck Collaboration XXIX (2014) describes in detail the selection method followed in the construction of the catalogue. The PSZ1 contains redshifts for 913 systems, of which 736 are spectroscopic. The purity depends on the S/N of the SZ detection, and is estimated to be ~95% for the entire PSZ1 sample.

PSZ2 is already publicly available (Planck Collaboration XXVII 2016). However, the optical follow-up presented here includes only PSZ1 sources (which will be targets for a forthcoming new study). Our long-term observing programme has recently been completed and we are analysing the data retrieved.

An initial effort at validating the PSZ1 sources (Planck Collaboration XXIX 2014) was made in order to search for SZ counterparts in optical data through the DSS[2] images, SDSS survey (SDSS, DR8, Aihara et al. 2011) and the *WISE* all-sky survey (Wright et al. 2010). In addition, the PSZ1 catalogue was cross-correlated with X-ray data, mainly with the ROSAT All Sky Survey (RASS, Voges et al. 1999, 2000), as well as other SZ catalogues. After these processes, the unconfirmed SZ sources were targeted for follow-up observations at the RTT150 telescope (Planck Collaboration Int. XXVI 2015), the Canary Islands observatories (this work and Planck Collaboration Int. XXXVI 2016), and the MegaCam at CFHT (van der Burg et al. 2016). Streblyanska et al. (2018) have very recently characterized 37 new *Planck* PSZ2 targets and presented updated redshifts for a sample of PSZ1 targets using the SDSS DR12 database.

---

[2] DSS: http://stdatu.stsci.edu/dss

Table 1. Telescopes and instruments at ORM used in this optical follow-up validation programme.

Telescope	Instrument	FoV	Pixel scale ["]	Resolution	N_{ima}	N_{spec}
2.5 m INT	WFC	$34' \times 34'$	0.33	–	42	–
3.6 m TNG	DOLORES	$8\rlap{.}'6 \times 8\rlap{.}'6$	0.252	$R = 600$	1	20
4.2 m WHT	ACAM	$8' \times 8'$	0.253	$R = 400$	71	2
10.4 m GTC	OSIRIS	$7\rlap{.}'8 \times 7\rlap{.}'8$	0.254	$R = 500$	–	26

Notes. Columns 3 to 5 show field of view, the pixel scale and the resolution used in the imaging and spectroscopic observing mode. The last two columns list the total number of clusters observed performing imaging and spectroscopy.

2.2. Optical follow-up observations

All observations were carried out at Roque de los Muchachos Observatory (ORM) on the island of La Palma (Spain) within the framework of the International Time Programme ITP13B-15A. The dataset was obtained in multiple runs from August 2013 to July 2014, as part of this two-year observing programme.

Table 1 lists the ORM instruments and telescopes used for this follow-up work: a) the 2.5 m *Isaac Newton* Telescope and the 4.2 m *William Herschel* Telescope operated by the Isaac Newton Group of Telescopes (ING); b) the 3.5 m Italian Telescopio Nazionale *Galileo* (TNG) operated by the Fundación Galileo Galilei of the INAF (Istituto Nazionale di Astrofisica), and c) the 10.4 m Gran Telescopio Canarias (GTC) operated by the Instituto de Astrofísica de Canarias (IAC).

Our targets are unknown PSZ1 clusters, which usually correspond to low S/N SZ sources in this catalogue. However, the observational strategy prioritizes targets with highest SZ S/N, with the sole restriction that targets have declinations $>-15°$, in order to be observable from the ORM. Targets with lower declinations are scheduled for other follow-up programmes to be developed from southern hemisphere facilities.

We searched for possible counterparts in the Sloan Digital Sky Survey (SDSS)[3] and the Digitized Sky Survey (DSS)[4]. After this previous screening, and depending on whether the cluster was confirmed as counterpart, new imaging was not needed and only spectroscopic observations were required. Galaxy cluster members for which SDSS spectroscopic information was available were also considered in order to compute the mean cluster redshift.

In short, after previous screening in archive and public data searches for possible SZ counterparts, our observational strategy followed two steps. First, cluster counterparts were identified using deep images and, if these existed (as galaxy overdensities), they were studied photometrically using g', r', and i' broadband filters. Second, clusters were definitely confirmed through spectroscopic observations, either using long-slit or multi-object spectroscopy (MOS). Finally, taking into account all the photometric and spectroscopic information, the cluster validation was then performed based on the selection criteria detailed in Sect. 3.

2.2.1. Imaging observations and data reduction

Imaging observations were carried out using the Wide-Field Camera (WFC) mounted on the 2.5 m INT and the auxiliary-port camera (ACAM) mounted on the 4.2 m WHT. We obtained images for every target in the g', r' and i' Sloan bands. The WFC camera at the INT is a four EEV $2\,k \times 4\,k$ CCD mosaic with a projected pixel scale of $0\rlap{.}''33$, giving a field of view (FOV)

of $34' \times 34'$. ACAM is mounted at the folded Cassegrain focus of the 4.2 m WHT, which provides a FOV of $4'$ radius with a projected pixel scale of $0\rlap{.}''25$.

The High Frequency Instrument (HFI) *Planck* maps extend from 100 to 857 GHz, and their beam FWHM varies from $9\rlap{.}'6$ at the lowest frequencies to $4\rlap{.}'5$ at the highest. The positional error of sources is about $2'$ for targets in the PSZ1 sample (Planck Collaboration XXIX 2014). This result has been confirmed by comparing *Planck* SZ and REFLEX II sources. For the 83 clusters that overlap in the two catalogues, Böhringer et al. (2013) found that 78% are found with a detection offset smaller than $2'$. Optical counterparts are therefore not expected to be found beyond 2.5 times the beam size, which means that the cluster associated with the SZ effect should be closer than $\sim 5'$ from the corresponding PSZ1 coordinate. However, when the clusters are nearby systems ($z < 0.2$) their apparent radius may fill a large region, and in these cases their centre offsets relative to their SZ position may be higher. So a typical field of $10'$ is large enough to cover the region in which counterparts are expected with respect to the nominal SZ *Planck* coordinates (Planck Collaboration XXIX 2014).

The fields observed using the WFC were acquired with 1500 s exposures per band and by performing a small dithering pattern of three points with about $10''$ offset. This technique allowed us to remove bad pixels and vignetting, correct most of the fringing effects that are present in the CCD, and minimize the effect of cosmic rays. An analogous procedure was applied in the ACAM acquisitions, with the only difference that the total integration time per band was 900 s, split into three separate exposures of 300 s. The completeness and limit magnitudes[5] computed from object counts in the r'-band obtained with these integration times were $r' = 23.2$ and 24.0 mag using the WFC, and $r' = 23.8$ and 24.9 mag in the ACAM frames, respectively.

The optical WFC and ACAM images were reduced using standard `IRAF` tasks[6]. The reduction procedure includes bias and flat-field corrections and astrometric calibrations. The astrometry was performed using the `images.imcoords` task and the USNO B1.0 catalogue as reference. The photometric calibration refers to SDSS photometry and SDSS standard fields. When the observations were carried out in non-photometric conditions, the targets were calibrated in the subsequent observing run under clear skies.

The source detection and photometry were performed using `SExtractor` (Bertin & Arnouts 1996) in single-image mode.

---

[3] http://skyserver.sdss.org
[4] http://archive.stsci.edu/dss

[5] Completeness and limit magnitudes correspond to detection targets with $S/N \sim 5$ and 3, respectively.
[6] IRAF (http://iraf.noao.edu/) is distributed by the National Optical Astronomy Observatories, which are operated by the Association of Universities for Research in Astronomy, Inc., under cooperative agreement with the National Science Foundation.

Sources were detected in each of the g'-, r'-, and i'-bands if they presented more than 10 pixels with $S/N > 1.5\sigma$ detection threshold in the filtered images. We performed elliptical aperture photometry with variable size using the MAGAUTO set-up. The parameters of the "Kron factor" and the "minimum radius" were set to the default values of 2.5 and 3.5, respectively. All the photometric catalogues were then merged in order to create a master catalogue containing the three-band photometries.

Unfortunately, the WFC presents large PSF distortions over the wide FOV. This implies that it was very difficult to classify faint sources ($r' > 18$ mag) as stars or galaxies. So, we performed star-cleaning procedures within small regions containing the cluster candidates in order obtain clear RS in the colour–magnitude diagrams.

2.2.2. Spectroscopic observations and data reduction

The majority of the data presented here was acquired using the DOLORES and OSIRIS spectrographs at the 3.5 m TNG and the 10.4 m GTC, respectively. However, in a few cases, ACAM (at the 4.2 m WHT) was also used in its spectroscopy mode. DOLORES and OSIRIS observing blocks were made in MOS mode while ACAM was set-up in long slit configuration.

We used the DOLORES spectrograph at the TNG. This instrument has a $2k \times 2k$ CCD detector with a pixel scale of $0.''252$. We performed low resolution spectroscopy using the LR-B grism (dispersion of $2.75\,\text{Å}\,\text{pixel}^{-1}$ in the range 4000–8000 Å) with slit widths of $1.''6$, yielding a resolution of $R \sim 600$. We placed about 40–45 slitlets per mask and acquired He-Ne and Hg-Ne arcs, which allowed us to obtain wavelength calibrations with $rms \sim 0.1$ Å over the whole wavelength range. We obtained three exposures of 1800 s per cluster in order to obtain spectra with $S/N \sim 5$ for galaxies with magnitudes $r' = 20.5$.

We used the OSIRIS spectrograph at the GTC in MOS observing mode. This instrument has a double $2k \times 4k$ CCD detector used with a binning of 2×2 pixels, which gives a final pixel scale of $0.''25$. We placed up to 60 slitlets per mask of $1.''2$ widths. The R300B grism was used in order to get a dispersion of $5.2\,\text{Å}\,\text{pixel}^{-1}$ ($R \sim 500$) over the full visible wavelength range. We obtained wavelength calibrations with $rms \sim 0.2$ Å accuracy using Hg, Ne, and Ar lamps. 3×1000 s exposures per mask were acquired in order to get spectra with $S/N \sim 5$ for galaxies with magnitudes $r' = 21.6$. For some specific targets we used the OSIRIS spectrograph in long-slit mode, using the same grism and slit width set-up as used for the MOS unit.

Both the DOLORES/TNG and OSIRIS/GTC masks used three to five pinholes as pivots placed on a fiducial star to centre the masks. The masks were designed using previous imaging for each field, and galaxies were selected from the photometry obtained with the WFC. Basically, we used RGB colour composite images as a reference and considered cluster members that galaxies contained within the RS of the cluster, obtained from $g' - r'$ and $r' - i'$ colours. This selection procedure yields a success rate of about 60% in the core of the clusters, and 20% in the external regions (>0.3 Mpc from the bright cluster galaxy, the BCG).

We used ACAM at the 4.2 m WHT telescope. This instrument also offers a long-slit spectroscopy mode. It is equipped with a $2k \times 2k$ CCD with a projected pixel scale of $0.''25$. The disperser is a holographic device offering a wavelength coverage between 4000 and 9000 Å, a dispersion of $3.3\,\text{Å}\,\text{pixel}^{-1}$ and a resolution of $R \sim 400$ for a slit width of $1''$. We obtained spectra for the BCG and several other cluster members by positioning the slit in two or more orientations. We used exposure times of 2×1000 s per slit in order to obtain spectra with $S/N \sim 5$ for galaxies with magnitudes $r' \sim 19.5$. We noticed that this spectrograph is not so efficient as other homologous devices, probably owing to its holographic disperser. We obtained lower S/N spectra, as expected for the chosen exposure times.

The data reduction included sky subtraction, extraction of spectra, cosmic ray rejection, and wevelength calibration. All these procedures were performed using standard IRAF tasks. After a careful test, we decided to do not apply bias and flat-field correction, because these corrections added unwanted noise to the low signal of the faint sources. The wavelength calibration of scientific spectra was performed using He-Ne, Hg, and Ar arcs. We then checked the calibrated spectra and looked for possible deviations using the OI telluric line (5577.3 Å). We found no systematic offsets, but random deviations of about 1 Å, which correspond to $\sim 50\,\text{km s}^{-1}$ with the instrument set-up used.

The reduced spectra showed $S/N \sim 5$ (per pixel around 5500 Å) for galaxies with $r' \sim 19.5$, 20.5, and 21.7 mag, observed with the WHT, TNG, and GTC respectively. Our observational strategy consisted in observing the nearby clusters ($z_{\text{phot}} \lesssim 0.4$) at the TNG and WHT, whereas the most distant systems ($z_{\text{phot}} \gtrsim 0.4$) were observed using the GTC. Figure 1 shows two examples of spectra obtained at the TNG and GTC.

The long-slit observations were planned in order to get the maximum number of redshift estimates by placing between two and four galaxies within the slit, and selecting two position angles for each cluster candidate. We always included the BCG in one of the position angles. Therefore, with this scheme we were able to obtain as many as five or six redshifts per cluster candidate.

We estimated radial velocities using the cross-correlation technique (Tonry & Davis 1979) implemented in the IRAF task RVSAO[7]. The science spectra were correlated with six spectrum templates (Kennicutt 1992) of various galaxy morphologies (E, S0, Sa, Sb, Sc, and Irr). The XCSAO procedure provides an R parameter linked with the S/N of the cross-correlation peak. We chose the radial velocity corresponding to the template with the highest R-value. Most of the redshifts were estimated using only absorption lines (mainly the H and K CaI doublet, G-band, and MgI triplet), as corresponds to a dominant early-type population of galaxies in clusters. However, a few cases showed strong emission lines (mainly OII, OIII doublet, and H_β), which were used to determine the redshift. Finally, we visually inspected all spectra to verify the velocity determination, which was particularly difficult for galaxies at $z > 0.7$, owing to the low S/N of the continuum of the spectra and the few spectral features identified within the visible wavelength range.

At the end of this process, the cross-correlation yielded a mean error in the radial velocity estimates of $\Delta v \sim 75\,\text{km s}^{-1}$. However, double redshift determinations for a set of about 50 spectra allowed us to estimate the true intrinsic errors. By comparing the first and second velocity estimates we obtained an rms of $\Delta v = 110\,\text{km s}^{-1}$. This means that actual errors in the redshift estimates are $\Delta z \sim 0.0004$, which is in agreement with the predicted value for the resolution set-ups of the spectrographs used in this study.

The multi-object masks allowed us to sample the core of the clusters in a more complete way. We obtained typically 40–50 radial velocities per mask and retrieved 10–25 galaxy

---

[7] RVSAO was developed at the Smithsonian Astrophysical Observatory Telescope Data Center.
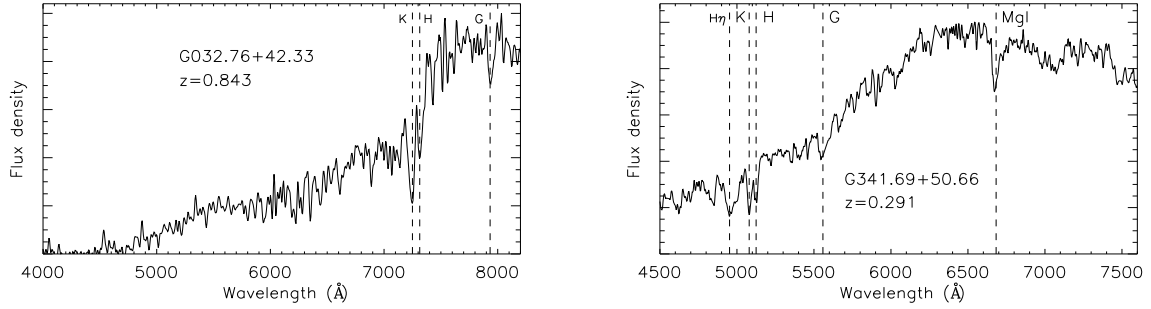
Fig. 1. Example of the spectra obtained with GTC/OSIRIS (*left panel*) and TNG/DOLORES (*right panel*) for two luminous galaxy members, with magnitudes $r' = 21.6$ and 17.8, in the clusters G032.76+42.33 and G341.69+50.66, at $z = 0.843$ and 0.291, respectively. Dashed lines correspond to the wavelength of the absorption features identified in each spectrum at the redshift of the clusters. Flux density is plotted in arbitrary units.

members per cluster, which means a success rate of about 20–50%. We estimated the mean redshift and velocity dispersion of the clusters. In all cases, the cluster redshift was assumed to be the mean value for the galaxy members retrieved.

In this study, we considered galaxy members only if they showed radial velocities of $\pm 2500 \, \mathrm{km \, s^{-1}}$ with respect to the mean velocity of the systems. Given that this range is about three times the typical velocity dispersion of a cluster, this criterion guaranteed that we selected the vast majority of galaxy members while minimizing contamination of interlopers.

3. Cluster identification and confirmation criteria

We identified clusters in the images as galaxy overdensities showing coherent colours. The significance of each overdensity is evaluated through the richness parameter R (see below), whereas colours and photometric redshifts are estimated on the basis of the red sequence (hereafter RS; Gladders & Yee 2000). We selected likely galaxy members using the cluster RS in the $(g' - r', r')$ and $(r' - i', r')$ colour–magnitude diagrams (CMD). We defined the RS as galaxies showing a coherent colour. That is, we looked for galaxies with similar colours around a bright one (assumed to be the BCG) in the observed region forming a compact group of galaxies in space. We fitted the RS by calculating the mean colour of the five brightest likely members and fixing the RS slope to -0.039 and -0.017 in $(g' - r', r')$ and $(r' - i', r')$ CMDs respectively (see Barrena et al. 2012). Thus, we combined the colour information of galaxy member candidates and their spatial distribution in order to search for galaxy overdensities, thus estimating the corresponding photometric redshift (see Fig. 2). We used the mean colour of the five brightest galaxies of the cluster to estimate the photometric redshift. The process we followed to estimate z_{phot} using the colours of the galaxy population is detailed in Planck Collaboration Int. XXXVI (2016, see Sect. 4.2, and Eqs. (1) and (2) therein). In addition, galaxies with colours within the RS ± 0.15 were considered as cluster member candidates and selected as galaxy targets for further spectroscopic observations.

We also used the g'-, r'-, and i'-band exposures to compose RGB colour images. These RGB (colour composite) frames were used to consolidate our findings. Therefore, actual galaxy overdensities were clearly identified by eye. This visual inspection proved to be very efficient for the identification of high redshift ($z > 0.7$) clusters, or even fossil systems. In the former, our optical data were not deep enough to identify the cluster RS, but the galaxy overdensities corresponding to the brightest members were clearly visible in the RGB images at the minimum detection level. On the other hand, fossil systems (e.g. Jones et al. 2003; Voevodkin et al. 2010) are very evolved structures with
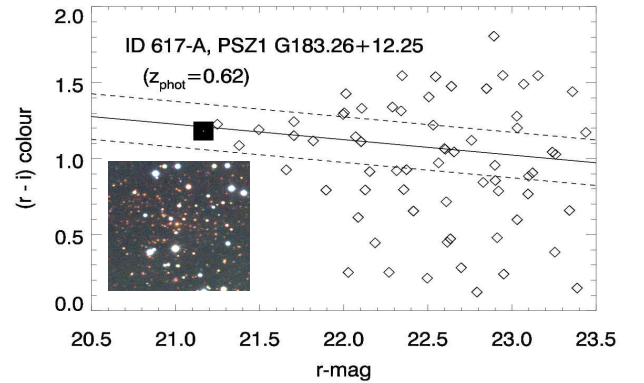

Fig. 2. $(r' - i', r')$ CMD of ID 617-A, associated with PSZ1 the source G183.26+12.25. The diagram considers extended sources within a region of 2.5×2.5 (1×1 Mpc) around the BCG of the system (represented by the large filled square in the plot). The solid line represents the fitted RS, which yields $z_{\mathrm{phot}} = 0.62$. Dashed lines correspond to the RS± 0.15 locus, where likely cluster members are selected. An RGB image (composed using the g', r' and i' frames) showing the 2.5×2.5 inner region of this cluster is superimposed on the plot.

a mass content capable of producing a detectable SZ effect on *Planck* maps (Pratt et al. 2016). These kinds of galaxy clusters, characterized by the presence of a huge central BCG and a poor galaxy population, are also particular cases that are not easily detected by automatic algorithms in colour space. Their RS are usually not very populated owing to the two-magnitude gap beyond the BCG, so these kinds of clusters do not fit the standard RS. Visual inspection of RGB images is therefore essential.

Confirmation criteria. In order to perform a robust confirmation of the PSZ1 sources, we adopted the criteria set out in Table 2. This set of conditions is based on the dynamical properties of the clusters (through their velocity dispersion retrieved from spectroscopic observations), richness, and distance from the *Planck* pointing. We therefore classified the counterparts with different flags according to the validation level of each target.

The mass–redshift distribution of the *Planck* cluster sample is reported in Planck Collaboration XXXII (2015), which provides the detectable mass of SZ sources in the PSZ1 catalogue. So, following this relation, one would expect that no poor systems are validated even if they are in the SZ line of sight. However, owing to the noise inhomogeneity in the *Planck* Y_{500} maps (Planck Collaboration XX 2014; see Fig. 4 therein), or statistical effects, relatively low-mass haloes may scatter beyond the SZ detection threshold. The statistical influence on detection samples is known as the Eddington bias (Eddington 1913). vdB+16 studied this effect on the measured SZ-based

Table 2. Confirmation criteria adopted to validate or reject clusters as counterparts of SZ detections.

Flag	Spectroscopy	σ_v limit (km s^{-1})	R (N_{gal})	Dist.
1	YES	>500 ; $0 < z < 0.2$	>15	$<5'$
		>650 ; $z > 0.2$	>15	$<5'$
2	NO	NA	>15	$<5'$
3	YES	<500 ; $0 < z < 0.2$	>15	$<5'$
		<650 ; $z > 0.2$	>15	$<5'$
	NO	–	>15	$>5'$
ND	–	–	≤ 15	–

masses and confirmed 13 SZ counterparts at $z > 0.5$ showing $M_{500} \gtrsim 2 \times 10^{14}$ $M_\odot$ h_{70}^{-1}. Moreover, nearby ($z < 0.2$) galaxy systems may also be detected in *Planck* SZ maps, some even showing masses $M_{500} \sim 10^{14}$ $M_\odot$ h_{70}^{-1}. Given that we have spectroscopic information for a reasonable number of members and clusters, we were able to determine the velocity dispersions, and use them to investigate whether they are poor or massive systems. According to the M_{200}–σ_v scaling adopted in Munari et al. (2013) and the M_{200}–M_{500} relation suggested by Komatsu et al. (2011, see Eq. (D.15) therein), we estimated that clusters at $z < 0.2$ with $M_{500} > 10^{14}$ $M_\odot$ h_{70}^{-1} should present $\sigma_v > 500$ km s^{-1}, whereas clusters at $z > 0.2$ with $M_{500} > 2 \times 10^{14}$ $M_\odot$ h_{70}^{-1} should show $\sigma_v > 650$ km s^{-1}. So we assumed these limits on σ_v in order to distinguish between actual and detectable systems by *Planck* and chance identifications not linked to the SZ effect.

R is the "richness" computed as the number of likely members (galaxies in the RS±0.15 mag locus, which represents the $\pm 3\sigma$ colour dispersion of RS at its brightest part) in g'-r' and r'-i' for clusters at $z \leq 0.35$ and $z > 0.35$, respectively, showing magnitudes in the range $[r'_{BCG}, r'_{BCG} + 3]$ within a projected region of 0.5 Mpc radius from the centre of the cluster (assumed to be the BCG) at the redshift of the cluster. Likely member counts were decontaminated from the field contribution, which was computed considering the full set of images, excluding the 0.5 Mpc radius regions containing the core of the clusters. So the richness was obtained from likely member counts after subtraction of a mean field contribution (as a function of the redshift).

Cluster optical centres are taken as the BCG position, and centres of clusters that show no clear BCG are supposed to be the position of the most luminous member (or likely cluster member in cases where we have only photometric information). We also adopted confirmation criteria based on the distance to the PSZ1 coordinates. The predicted centre error for the whole PSZ1 is 2' (Planck Collaboration XXIX 2014), so we considered only those clusters at $<5'$ from the nominal position, which is a $>2.5\sigma$ position error with respect to the SZ peak emission, to be valid optical counterparts.

Therefore, following these three criteria based on velocity dispersion, richness and distance (see Table 2), definitely confirmed optical counterparts are classified with Flag = 1, which are massive, rich, and well centred systems (this subset includes ACO and Zwiky clusters); clusters potentially validated are classified as Flag = 2, which includes clusters that are well aligned with the *Planck* pointing with a few galaxy members spectroscopically confirmed or targets with no spectroscopy yet available (NA ≡ "not available" in Table 2) but rich from

the optical point of view; and Flag = 3 corresponds to clusters very marginally associated with their corresponding SZ signal owing to their low σ_v or large distance ($>5'$) with respect to the PSZ1 centre. In addition, the "non-detections" (ND) are, in practice, areas with an R compatible with the field galaxy count level, where no galaxy concentration is detected. We note that some SZ targets classified as ND report a galaxy system. In these cases, we wanted to enhance the existence of a galaxy system, but too poor, showing an R value to low ($R < 15$), or even very low σ_v, to be considered actual SZ counterpart under the restrictions imposed above.

In the majority of the cases, the analysis of the validation process following the confirmation criteria was unequivocal. However, in some fields, we found two or more separate systems, for which we obtained multiple photometric redshifts, which correspond to projection effects along the line of sight. These are multiple detections. In addition, we detect clusters with multiple clumps of galaxies assumed to be substructure (subclusters) of a single system. All these particular cases were investigated in detail by combining spectroscopic, photometric, and RGB images in order to disentangle the most probable counterpart for each SZ source. Following this scheme, we consider as "confirmed" optical counterparts those clusters classified with flag = 1 and 2, and "unconfirmed" targets to be those associated with flag = 3 and an ND label.

4. Results

Table A.1 lists the 115 clusters from the PSZ1 catalogue explored in our optical follow-up. The first column shows the index number in the PSZ1 list. The second column lists the corresponding named in the PSZ1 catalogue. Column 3 is the SZ significance reported in the PSZ1 catalogue. Columns 4, 5, and 6 are the J2000 equatorial coordinates corresponding to the most luminous cluster member (the BCG in most cases) and the distance between the optical and SZ centres. The multiple Col. 7 lists the mean spectroscopic redshift and the redshift of the BCG (if observed). Columns 8, 9, and 10 show the number of cluster members with spectroscopic measurements, the photometric redshift, and optical richness, respectively. Column 11 lists the cluster classification following the flag scheme described in Table 2, and Col. 10 adds some comments relative to other possible identifications or noteworthy features.

In accordance with Sect. 2.2.2, $z_{spec,BCG}$ values present a mean error of $\Delta z = 0.0004$. However, the error in $\langle z_{spec} \rangle$ is a bit higher, $\Delta z = 0.001$, owing to the particular features of each cluster member sample, such as the influence of the number of members considered, the 2D spatial distribution, presence of substructure and interlopers, amongst others.

Following the confirmation criteria given above, we find that 53 SZ sources have reliable optical counterparts, 25 of them classified with Flag = 1 and 28 with Flag = 2. In addition, we classified 49 PSZ1 sources as ND and 13 as being weakly associated with the corresponding SZ source (Flag = 3). This means that a total of 62 SZ sources in this sample remain unconfirmed.

We report 56 spectroscopic redshifts, 30 of them found using the MOS mode of the TNG and GTC. Three of these SZ sources show multiple optical counterparts. The physical magnitudes associated with these cluster counterparts, such as radial velocities of cluster members, velocity dispersions, and dynamical masses, will be discussed in detail in a future paper (Ferragamo et al. 2018 in prep.).
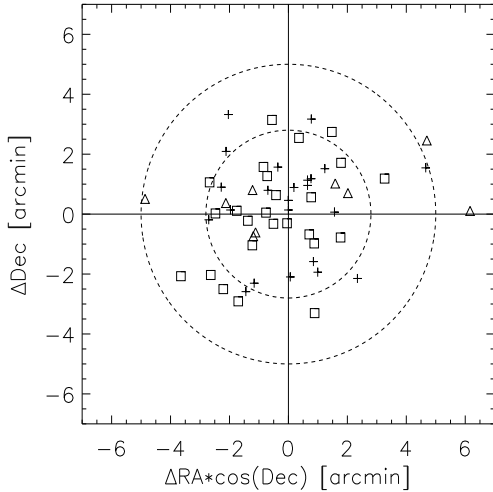
Fig. 3. Relative positions of optical counterpart centres respect nominal PSZ1 coordinates for clusters in Table A.1 flagged as "1" (crosses), "2" (squares), and "3" (triangles). Only optical counterparts with multiple detections are excluded. The inner dashed line show the region (of $2.\!'8$ radius) enclosing 68% of the confirmed clusters (flagged as "1" and "2"). The external dashed line corresponds to 2.5 times the beam size $(5')$ of *Planck* SZ detections.

In the following subsections, we analyse the precision of the SZ coordinates and the agreement between photometric and spectroscopic redshifts, and we discuss the nature of some of the clusters, in particular those systems presenting multiple optical counterparts and fossil systems. Finally, we study the presence of galactic dust as the most likely source of contamination in non-detections of SZ targets.

4.1. Precision of SZ coordinates and redshifts

Figure 3 shows the spatial distribution of the optical centres of clusters relative to the PSZ1 coordinates. Multiple optical counterparts have been excluded from this analysis. For these particular cases, it is difficult to determine a single optical centre and how individual clusters contribute to the SZ emission. Twenty-five clusters in our sample containing 54 actual optical counterparts are closer than $2'$ to the *Planck* SZ coordinate. In fact, 68% of the clusters are enclosed within $2.\!'8$, which is in agreement with the value of $2'$ predicted for the whole PSZ1 and found in the REFLEX II *Planck* SZ sources.

Figure 4 shows a similar analysis, where we plot the relative distance between the optical and SZ centres as a function of cluster redshift. Clusters at low redshift ($z < 0.1$) present larger apparent radii, so, at this redshift, a typical virial radius of 1 Mpc extends to about $10'$. This means that SZ–optical associations at $5-10'$ distance could be expected. However, we find no optical counterparts at large distances. Even in the cases of clusters at $z < 0.1$ the SZ–optical distance is below $5'$.

A comparison between photometric and spectroscopic redshifts for the clusters listed in Table A.1 is shown in Fig. 5. Photometric redshifts are estimated as described in Sect. 3. Clusters with $z > 0.75$ are excluded from this analysis because at this redshift range even the $r' - i'$ colour is unusable to determine reliable photometric redshifts. For clusters at $z > 0.75$ we would need photometry in the z'-band or even redder filters, which were not obtained in our imaging survey. Therefore, for clusters at $z_{spec} > 0.75$, the photometric redshift is expected to be lower than the actual value (see Fig. 5). This study yields a photometric
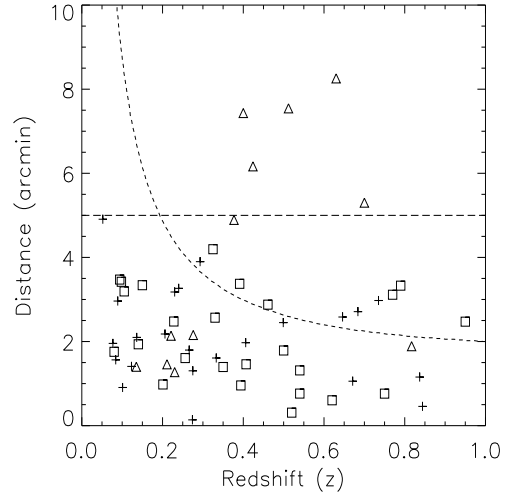

Fig. 4. Cluster optical centre offsets relative to their *Planck* SZ position as a function of cluster redshift. The dashed horizontal line at $5'$ shows the maximum offset expected for a *Planck* SZ detection (i.e. a *Planck* beam). The dotted line corresponds to the angle subtended by 1 Mpc in projection at the corresponding redshift. Symbols used are as in Fig. 3.
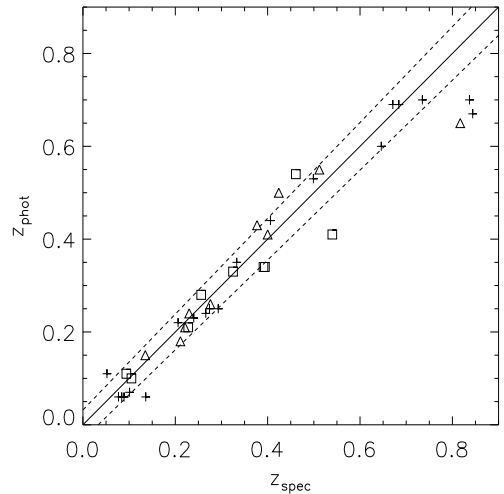

Fig. 5. Comparison between photometric estimates and spectroscopic redshifts. The continuum line represents the 1:1 relation and dashed lines show the photometric redshift error $\delta z/(1 + z) = 0.03$ when comparing clusters with $z < 0.75$. Symbols used are as in Fig. 3.

redshift error of $\delta z/(1 + z) = 0.03$ when comparing clusters with $z < 0.75$.

4.2. Notes on individual clusters

In this section, we present a detailed description of all the clusters in Table A.1 that show particular features, such as multiple detection targets, substructural evidence of non-relaxation, fossil systems, or massive clusters with strong lensing effects. The SZ counterparts not discussed in this section seem to be regular clusters that do not present any difficulty in their association with the corresponding SZ signal or any peculiarity from the optical point of view. We also compare here identifications with other optical confirmations of *Planck* PSZ1 sources. We note that all sky images presented in this section are orientated with north up and east to the left.

PSZ1 G028.01+25.46. We identify two possible counterparts, which we call clumps A and B, for this SZ source (see Fig. 6).
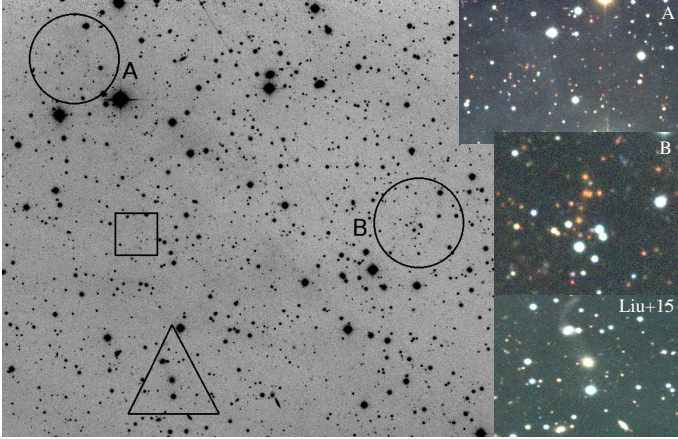
Fig. 6. Image obtained in the *r*-band with the WFC/INT for the PSZ1 G028.01+25.46 source covering a field of view of $10' \times 10'$. Circles A and B mark the respective positions identified in this article of these clumps at $z = 0.658$ and $z_{phot} = 0.60$. The square points to the *Planck* PSZ1 coordinates, and the triangle is located on the Liu+15 counterpart for this PSZ1 source. RGB colour images show magnified regions in each clump. We note that, from our photometric analysis, we do not detect any important concentration of galaxies with $z_{phot} = 0.284$ around the Liu+15 coordinates.

The A clump seems to be the richest counterpart. We performed multi-object spectroscopy using OSIRIS/GTC around clump A, and we confirmed this cluster by selecting nine cluster members at $z = 0.658$, showing a $\sigma_v \sim 900\,\mathrm{km\,s^{-1}}$. Clump B also shows a concentration of galaxies (poorer than clump A) with $z_{phot} = 0.60$ but remains at $6'$ from the *Planck* pointing. Consequently, we classify clump B as `Flag = 3`. Liu et al. (2015, hereafter Liu+15), using the Pan-STARRS Survey (Magnier et al. 2013), report an optical counterpart at $z_{phot} = 0.284$ around $RA = 17:11:45$ and $Dec = +07:15:17$. Nevertheless, we do not detect any important concentration of galaxies at this redshift around the reported location, except for a few galaxies that may configure a small system. Clump A is therefore the only reasonable (and massive) cluster associated with the PSZ1 G028.01+25.46 source, which we classify as `Flag = 1`, despite its centre being $5'.2$ (slightly $> 5'$) from the PSZ1 coordinates.

PSZ1 G032.15−14.93, PSZ1 G042.96+19.11, PSZ1 G065.13+57.53, and PSZ1 G108.26+48.66. These systems are clusters at $z = 0.377$, 0.499, 0.684, and 0.671, respectively. We confirm these systems photometrically and spectroscopically. We performed MOS using OSIRIS/GTC and we selected 10, 8, 20, and 29 galaxy members for each system, respectively. The analysis of the spatial distribution of likely cluster members, retrieved from WFC/INT data, shows evidence of the presence of substructures. PSZ1 G032.15−14.93 shows a peak around $RA = 19:43:11$, $Dec = −07:24:56$, which represents the main body of the system, with $\sigma_v \sim 550\,\mathrm{km\,s^{-1}}$, and a secondary peak, at $4'$ towards the west, which corresponds to 1.2 Mpc at the redshift of the cluster. PSZ1 G042.96+19.11 and PSZ1 G065.13+57.53 also present a bimodal configuration. These objects were observed with ACAM/WHT. Analysis of the 2D galaxy distribution suggests a secondary substructure at 0.8 Mpc ($2'.3$) towards the south-east of the centre of the cluster, whereas the PSZ1 G065.13+57.53 substructure is located at $5'$ (2.7 Mpc) in the north-east with respect to the main body of the cluster. The global σ_v of this cluster seems to be about 720 and $870\,\mathrm{km\,s^{-1}}$, respectively. PSZ1 G065.13+57.53 is one of the

richest clusters found in this study. Finally, PSZ1 G108.26+48.66 is more complex, showing three peaks in the 2D galaxy density distribution. We identify a main body in the central position and two substructures almost aligned with the east–west direction (see Fig. 7). From the radial velocities we estimate a global $\sigma_v \sim 970\,\mathrm{km\,s^{-1}}$.

PSZ1 G044.92−31.66. Liu+15 validate this cluster as an actual counterpart. However, after analysing our MOS data, obtained with DOLORES/TNG, we find only a very poor galaxy system showing a low velocity dispersion ($\sigma_v < 500\,\mathrm{km\,s^{-1}}$). We therefore classify this system as `flag = 3`, so that it is only very marginally associated with the SZ eource.

PSZ1 G075.29+26.66. This is a case of multiple detection. We selected two clusters within $6'$ of the *Planck* pointing. We map this region using WFC/INT and select two galaxy overdensities, the first with a redshift of $z = 0.282$ at $5'$ towards the south of the *Planck* pointing, and the second system with a estimated $z_{phot} = 0.30$ located at $5'$ towards the NE. We perform MOS with DOLORES/TNG around $RA = 18:08:44.26$ and $Dec = +47:41:09$ and we find ten cluster members showing $\sigma_v \sim 1000\,\mathrm{km\,s^{-1}}$. Even though both clusters are farther than $5'$ from this PSZ1 target's coordinates, we consider these two systems as actual counterparts of the SZ signal. In this case, the SZ peak is located very close to the intermediate point between the two clusters and, in this situation, the *Planck* SZ signal could be a combination of the individual SZ effects produced by the two clusters.

PSZ1 G081.56+31.03. This is an SZ target invalidated by vdB+16 owing to its low richness. The coordinates of the centre reported in Table A.1 differ from those listed in vdB+16 by less than $1'$. The reason for this difference is probably that vdB+16 estimate the cluster centre as the location that maximizes the richness measurement, whereas our coordinates refer to the position of the brightest cluster member. This counterpart, classified as `Flag = 2` by us, and that reported by vdB+16 correspond to the same galaxy distribution with photometric redshift estimates in agreement to within errors. Spectroscopic observations are
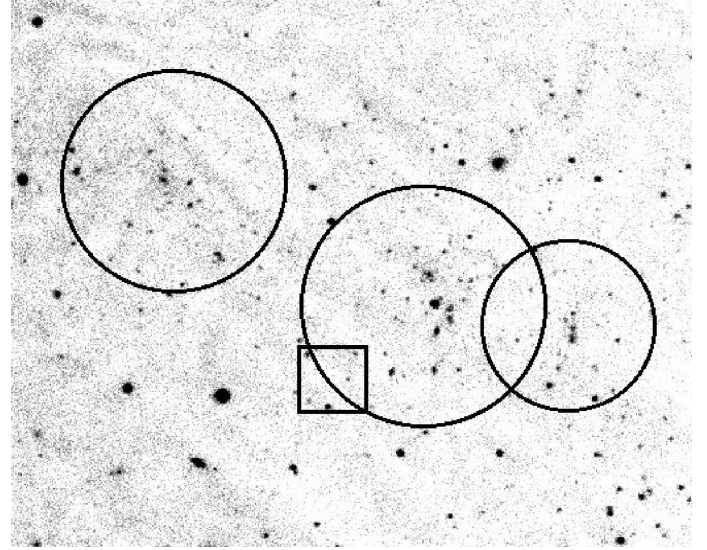

Fig. 7. *i*-band image, obtained with the WFC/INT, covering a $5' \times 4'$ FOV around the PSZ1 G108.26+48.66 cluster. Circles identify peaks in the galaxy density distribution consistent with $z = 0.671$. The square represents the *Planck* pointing of this SZ source.
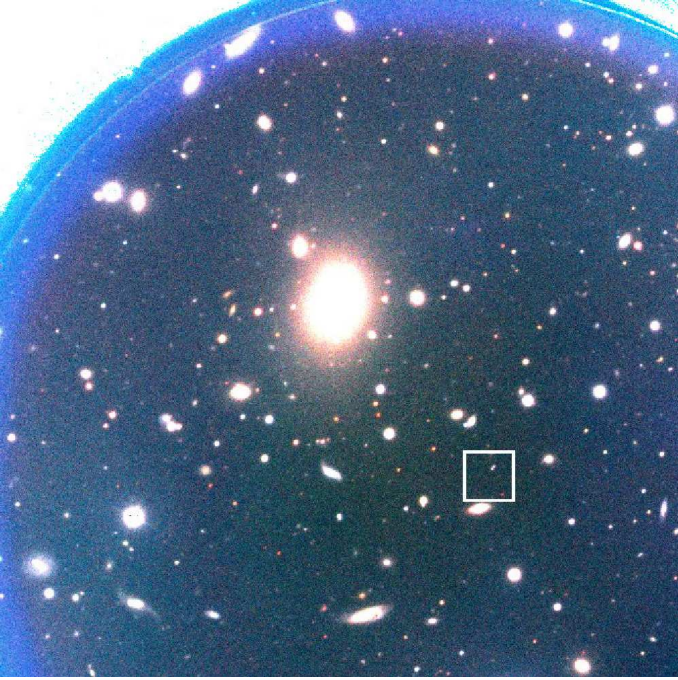
Fig. 8. Colour composite RGB performed using *g*-, *r*-, and *i*-band images of the cluster PSZ1 G103.94+25.81 covering an area of $5\farcm5 \times 5\farcm5$ FOV. The huge BCG is clearly visible at $2'$ to the NE of the *Planck* PSZ1 coordinates (square).

Fig. 9. PanSTARRS colour RGB image (composed of g', r', and i' filters) covering a $15' \times 13'$ FOV around the PSZ1 G142.1+157+37.28 source. The cross and the dashed line circle correspond to the PSZ1 nominal pointing and $5'$ selection area respectively. The cluster counterpart proposed in this study (at $z = 0.240$) and that proposed by Liu+15 (at $z_{\rm phot} = 0.284$) are marked by solid rectangles. Superimposed, an ACAM/WHT magnified image of the northern cluster is shown.

needed in order to clarify whether this cluster is a massive system or not.

PSZ1 G090.48+46.89. We detected two systems around this SZ target. First, we found a clump with $z_{\rm phot} = 0.54$ at $4'$ to the south of the *Planck* pointing. This is probably the only system associated with this SZ target. However, we detected a high-z system ($z = 0.676$) at a distance of $9'$ to the east, by selecting six cluster members using OSIRIS/GTC MOS around $RA = 15:44:07$ and $Dec = +57:46:43.2$, which seems to be too far from the *Planck* SZ coordinates.

PSZ1 G103.94+25.81 and PSZ1 G185.93−31.21. These are two clear fossil galaxy systems. ACAM/WHT images (see Fig. 8) reveal huge BCGs at $2'$ and $4'$ to the north-east of their respective *Planck* PSZ1 coordinates. We confirmed these systems spectroscopically by selecting 17 and 2 cluster members at $z = 0.077$ and 0.094 respectively. PSZ1 G103.94+25.81 shows $\sigma_{\rm v} \sim 650\,{\rm km\,s^{-1}}$.

PSZ1 G125.54−56.25. This is also a very complex region. We detected two clusters at $2'$ to the west of the *Planck* PSZ1 coordinates, labelled ID-458a and ID-458b in Table A.1. These two systems almost overlap on the sky plane and their BCGs present $z = 0.5475$ and $z = 0.1676$. In addition, we selected a third system, ID-458c, at $3\farcm4$ to the north of the *Planck* pointing. The three clusters present similar richness and all of them are placed at $<5'$ from the PSZ1 coordinates. They therefore probably all contribute to the SZ signal. The 2D galaxy distribution and photometric redshift have been derived from our ACAM/WHT images, and spectroscopic redshifts were obtained from the SDSS DR12 database.

PSZ1 G142.1+157+37.28. In this case, we find a discrepancy with Liu+15, who select a cluster counterpart for this SZ source with $z = 0.28$ located $6\farcm3$ to the SE of the *Planck* PSZ1
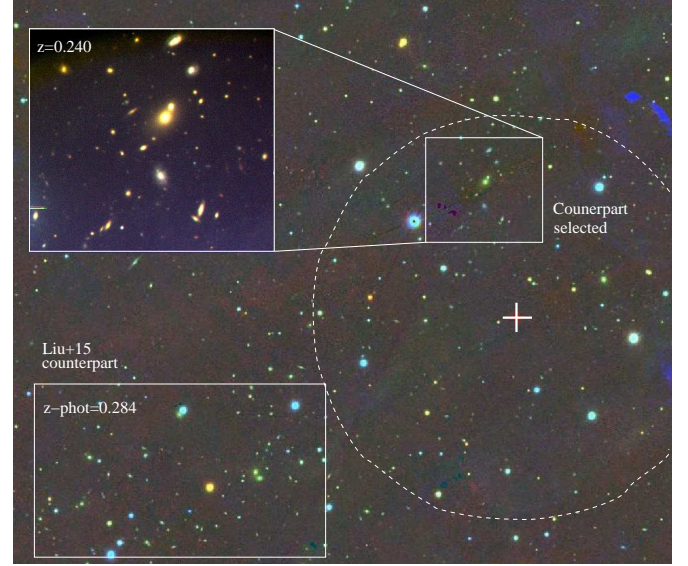
coordinates. However, we detected a different system located at only $3'$ to the north of the *Planck* pointing. With the MOS observations using DOLORES/TNG we confirmed this cluster by selecting six galaxy members at $z = 0.240$. From these few radial velocities, we derived a relatively high velocity dispersion, $\sigma_{\rm v} > 700\,{\rm km\,s^{-1}}$, which indicates that this system is massive and associated with the *Planck* SZ signal. It remains unclear whether the ID-508 cluster of Liu+15 can also be considered an actual counterpart of this SZ source. However, another possibility is that both clusters are gravitationally bound.

PSZ1 G151.80−48.06, PSZ1 G157.44+30.34 and PSZ1 G188.36−35.00. These three targets are known clusters, catalogued in Planck Collaboration XXIX (2014), Planck Collaboration XXXII (2015), and Abell et al. (1989) identified by correlating *Planck* PSZ1 sources with other known cluster catalogues. The three targets are ACO 307 (Abell et al. 1989), RX J0748.6+5940 (Appenzeller et al. 1998), and ZwCl 0401.8+0219 (Zwicky et al. 1961) respectively. However, their spectroscopic redshifts have been so far unknown. For that reason we obtained long-slit spectroscopy of the brightest galaxies of these systems. The two clear BCGs of ACO 307 present $z_{\rm spec} = 0.1999$ and 0.2011. For both RX J0748.6+5940 and ZwCl 0401.8+0219 we obtain four radial velocities of cluster members for each system, resulting in mean spectroscopic redshifts of $z = 0.407$ and 0.275 respectively.

PSZ1 G169.80+26.10. This is a complex region showing multiple counterparts. We detected two well separated systems at high redshift ($z_{\rm phot} = 0.73$ and 0.83 for A and B systems respectively) within $4\farcm2$ of the *Planck* pointing. We observed this region using WFT/INT adding the z' band to the g', r', and i' Sloan filters. This allowed us to make a better estimate of the photometric redshift, in particular for these high redshift clusters. Spectroscopy is needed in order to determine the precise redshift and σ_v of this system. However, the richness estimates agree with
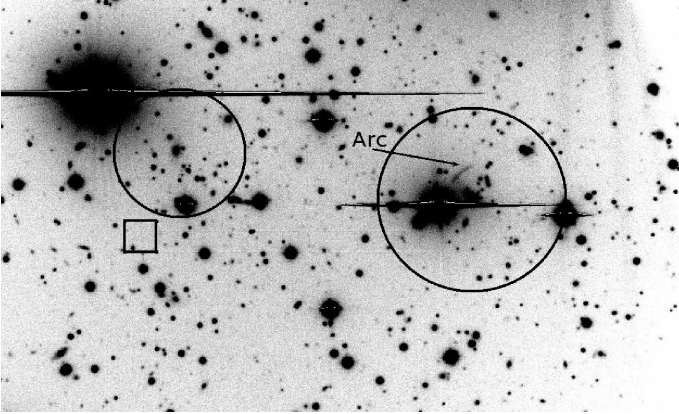
Fig. 10. $3' \times 5'$ *r*-band image of the cluster PSZ1 G206.45+13.89 obtained with ACAM/WHT. A large gravitational arc, marked with an arrow in the plot, is clearly visible around the BCG. Circles mark the core of the main body of the cluster (to the west) and the substructure, detected in the 2D spatial distribution of galaxies and radial velocities. The box indicates the *Planck* PSZ1 coordinates of this SZ target.

actual galaxy clusters. Thus, given that these two systems are enclosed in a small projected region on the sky and very close to the PSZ1 coordinates, they probably both contribute to the SZ signal of this PSZ1 source.

PSZ1 G183.26+12.25. We also classify this target as a multiple detection source. Two systems are identified at $z_{phot} = 0.27$ and $z = 0.638$ (see Fig. 2). Both systems present similar richness and are inside the $5'$ region of the *Planck* pointing, so the SZ signal of this PSZ1 source is probably a combination of the individual SZ effects produced by these two clusters. More spectroscopic observations are needed in order to estimate σ_v.

PSZ1 G206.45+13.89. This is the only cluster in our sample with strong lensing effects. We detect a significant gravitational arc around the BCG that is clearly visible in the cluster core (see Fig. 10). We performed MOS using OSIRIS/GTC and select 45 cluster members. The BCG is at $z_{BCG} = 0.4055$, and the global σ_v is ~ 1200 km s^{-1}, which shows that this is a massive cluster. Moreover, the 2D galaxy distribution and the velocity field of this cluster show evidence of dynamical non-relaxation and the presence of substructure. The subcluster coincides very well with the *Planck* PSZ1 coordinates, and the main body of the cluster is $2'.3$ to the west of the *Planck* pointing.

PSZ1 G341.69+50.66. This is a cluster selected by Liu+15 as a multiple detection. We obtained deep imaging with ACAM/WHT and performed MOS observations with DOLORES/TNG, retrieving more than 70 redshifts of galaxies in this field. Analysis of the velocity field of the galaxies reveals only one cluster at $z = 0.293$. We identified 31 galaxy cluster members and a global velocity dispersion of ~ 800 km s^{-1}, showing clear evidence of dynamical non-relaxation. The main body, which contains the brightest galaxies and the densest galaxy distribution, is located at $4'$ to the north-west of the *Planck* PSZ1 coordinates. The secondary substructure is placed at $RA = 14{:}25{:}34.54$ and $Dec = -05{:}00{:}34.3$, which corresponds to a distance of 2 Mpc from the main body at the redshift of the cluster. So, the *Planck* PSZ1 target is at the mid-point bewteen the main body and substructure positions, but we did not identify multiple counterparts in this SZ source.

4.3. Non-detections and comparison with other previously studied counterparts

The validation criteria described in Sect. 3 yield 62 SZ sources classified as ND or as clusters weakly associated with the SZ signal detected by *Planck*. This means that no cluster counterparts were detected for 54% of the sample, where our deep imaging and spectroscopic data did not show any evidence of optical counterparts to the SZ sources. There are two possible ways to explain these non-identifications. The first and most plausible explanation is that there is no optical counterpart, owing to false SZ detections, high noise in the Y_{500} *Planck* maps (Planck Collaboration XX 2014; see Fig. 4), or contamination in SZ maps produced by radio emission of galactic dust clouds. A second explanation is that the cluster counterpart does exist but is at high redshift ($z > 0.85$), hence making it very difficult to detect at visible wavelength.

In addition, we detected a few discrepancies with respect to previously reported counterpart validations. Whereas, overall, we fully agree with VdB+16 validation, Liu+15 validate some clusters as actual counterparts that we classify as ND and `Flag = 3`. The reason behind these disagreements is probably the different methods and restrictions imposed to validate counterparts. In the following, we discuss the nature of some non-confirmed clusters in order to contextualize this kind of classification (`Flag = 3` and ND).

PSZ1 G031.41+28.75. vdB+16 studied this SZ source as a cluster with $z_{phot} = 0.42$, a richness of $R = 20.9 \pm 7.4$, and a Richness Mass[8] of M $= 1.07 \pm 0.4 \ 10^{14} \ M_\odot$, located at $4'$ towards the west of the *Planck* pointing. However, vdB+16 invalidate this counterpart owing to its low richness mass. In agreement with vdB+16, we do not detect any significant galaxy concentration within a region of $5'$ radius from the *Planck* pointing, consistent with this photo-z. However, we detect a poor galaxy overdensity almost aligned with the PSZ1 coordinates and showing a coherent colour distribution in agreement with $z_{phot} = 0.24$. Long-slit spectroscopy observations, using OSIRIS/GTC, for four galaxy members confirmed this galaxy system to have a redshift of $z = 0.230$, but more spectroscopic observations are needed in order estimate its σ_v so as to consolidate its validation as actual counterpart. For the moment, we classify this cluster as a very marginal counterpart (`Flag = 3`) because of its low richness.

PSZ1 G078.39+46.13. This is an SZ target studied by Liu+15, using SDSS DR12 data, we also identify this cluster at $<z_{spec}> = 0.400$ and located at $7'.5$ to the south of the *Planck* pointing. Liu+15 validated this cluster as an actual counterpart. However, following our validation criteria, we found this cluster to be too far from the PSZ1 coordinate to be considered a realistic counterpart. We therefore classified this cluster with `flag = 3`, indicating a weak association with this SZ target. No additional galaxy overdensities were found within the region of $5'$ radius.

PSZ1 G135.92+76.21. We have performed MOS using OSIRIS/GTC and DOLORES/TNG and retrieved more than 80 redshifts in this region. Among this spectroscopic sample, we detected two systems. One of them at $z_{spec} = 0.406$ and a second at $z_{spec} = 0.767$ (around $RA = 12{:}35{:}24.10$, $Dec = +40{:}30{:}08.02$; these have not been included in Table A.1 as a multiple detection). We detected 9 galaxy members in the former, and 11 members in the latter. However, the dynamical analysis reveals a

---

[8] The richness mass is the mass of the cluster estimated from the mass–richness relation of Rykoff et al. (2014) and Rozo et al. (2015).
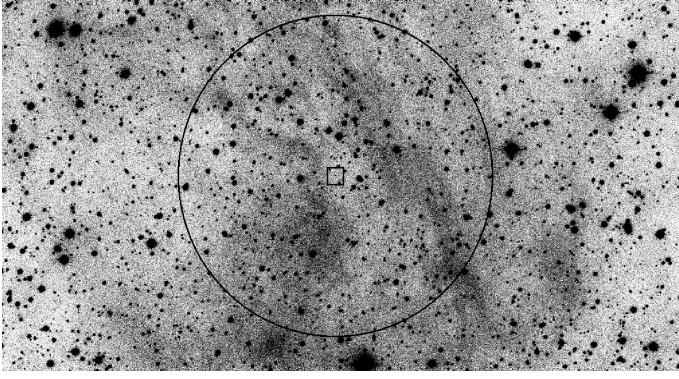
Fig. 11. WFC/INT *g*-band image of the target PSZ1 G001.00+25.71. The square marks the PSZ1 position, and the circle encloses the 5′ region around the *Planck* pointing. No cluster counterpart is identified in this case. The presence of significant galactic gas and dust structures may have influenced the SZ detection in this area.

$\sigma_v < 500\,\mathrm{km\,s^{-1}}$ and the optical richness is also $R < 15$ in both two cases. So, despite these two systems' possibly configuring actual galaxy groups, they are too poor and non-massive to be associated with the SZ emission.

Galactic cirrus is common in targets of low galactic latitude. In fact, we detected large dust and gas structures in the images of the majority of our targets. Moreover, the presence of gas and dust galactic filaments is even very common in pointings at $|b| > 25°$ but close to the galactic centre ($300° < l < 60°$; see Fig. 11). Half of the sample (57 clusters) are targets with $|b| < 25°$, of which 32 are classified as ND and only three with `Flag = 3`. These numbers reveal that about 61% of them are unconfirmed SZ targets located close to the galactic plane.

On the other hand, taking into account targets with $|b| > 25°$, we classify 27 (47%) sources as not confirmed (ND+"3"), while we detect 31 (53% of confirmed clusters) of positive ("1"+"2") optical counterparts. Therefore, even though the optical follow-up presented here is incomplete, the numbers are indicative of the low purity of PSZ1 catalogue for targets with low SZ significance. In addition, we see a higher fraction of unconfirmed sources at $|b| < 25°$, which suggests that targets located close to the galactic plane are more likely to present dust contamination or even high SZ detection noise.

PSZ1 G053.50+09.56. This is a low galactic latitude field and is therefore crowded with stars. This makes the detection of faint galaxies in the background very difficult. vdB+16 select this cluster, located at 4′ to the south of the PSZ1 coordinates at $z_\mathrm{phot} = 0.12$ with very low richness mass, $M \sim 10^{13}\,M_\odot$. vdB+16 consequently discount this cluster as realistic SZ counterpart. In agreement with this result, we do not detect any galaxy concentration with consistent photo-z in this field, we classify this target as an ND.

PSZ1 G052.93+10.44 and PSZ1 G286.25+62.68. These are two special cases. Photometric data obtained with WFC/INT show the presence of galaxy densities well aligned with the *Planck* pointing with $z_\mathrm{phot} = 0.24$ and 0.18 respectively. In fact, after obtaining DOLORES/TNG MOS data, we confirmed these clumps as actual systems, retrieving ten and eleven galaxy members for each cluster respectively. However, the radial velocities obtained show a low σ_v. Both structures present $\sigma_v < 350\,\mathrm{km\,s^{-1}}$. So, although PSZ1 G052.93+10.44 and PSZ1 G286.25+62.68 present optical counterparts, the corresponding

galaxy systems are probably very poor, being more group-like structures and hence very unlikely to be able to generate a significant SZ signal in *Planck* maps. These cases illustrate how chance alignments of poor clusters with SZ targets may introduce false identifications in SZ counts and how spectroscopy is the only way for revealing the actual nature of clusters by clarifying whether mass and σ_v take reasonable values to generate a detectable SZ signal for *Planck* instruments.

PSZ1 G050.01−16.88, PSZ1 G098.67−07.03, and PSZ1 G345.81+42.38. We inspected these SZ targets using WFC/INT and ACAM/WHT deep images and detected a few not very prominent galaxy concentrations, but with a coherent z_phot and resembling galaxy clusters. However, after performing OSIRIS/GTC and DOLORES/TNG spectroscopy and analysing more than 40 radial velocities of galaxies in each field, we did not select any actual cluster within these regions. The images of PSZ1 G050.01−16.88 and PSZ1 G098.67−07.03, as low galactic latitude sources, reveal the presence of diffuse galactic dust and gas.

PSZ1 G071.64−42.76. This PSZ1 source was studied by vdB+16, who invalidated this counterpart. This source shows the highest SZ significance ($S/N = 8.82$) of all the targets included in this study. In agreement with vdB+16, the WFC/INT images do not show any significant galaxy overdensity. Only a very poor group of galaxies at $RA = 22{:}30{:}50.00$ and $Dec = +05\,39\,16.72$ compatible with $z_\mathrm{phot} = 0.69$ is found. This region shows evidence of galactic dust contamination that is clearly visible in the *g*-band images. We therefore classify this PSZ1 target as ND. This case illustrates how the PSZ1 catalogue is not completely pure and how even high S/N SZ sources may be false SZ detections.

A few cases are very representative of how SZ detection with high SZ significance can be associated with low-mass galaxy clusters. For example, PSZ1 G108.90−52.04, PSZ1 G157.44+30.34, and PSZ1 G148.20+23.49 reveal SZ $S/N > 6.8$ but with $R < 40$. On the contrary, PSZ1 G206.45+13.89 and PSZ1 G224.82+13.62 show very high optical richness ($R > 120$) but moderate SZ S/N (<6). Optical richness, R, and SZ significance do not necessarily have to be correlated. This non-correlation can be explained in terms of the presence of galactic dust whose contribution contaminates the *Planck* SZ detection, the Eddington bias in this sample, and noise inhomogeneities in the *Planck* maps.

PSZ1 G090.14−49.71. Liu+15 validate this SZ source with a cluster at $z_\mathrm{phot} = 0.207$ located 13′.2 from the PSZ1 coordinates. Following our selection criteria, we find no significant galaxy concentration in the ACAM/WHT images showing coherent z_phot within 5′ from the PSZ1 position. Thus we classified this SZ target as ND.

5. Conclusions

This article is a continuation paper of the *Planck* validation catalogue of SZ sources (PSZ1) published in Planck Collaboration Int. XXXVI (2016). The work presented here shows the results of the first year of observations of the ITP13B-15A at the ORM, using the INT, TNG, WHT and GTC, as part of the optical follow-up validation and characterization programme of SZ *Planck* sources.

We studied 115 SZ sources based on deep imaging and spectroscopy, which allowed us to analyse, in an unbiased way, the nature of systems based on their 2D galaxy distribution, and

radial velocities. By using photometric and spectroscopic observations we adopted a robust counterpart classification based on the alignment with respect to the *Planck* SZ coordinates, the optical richness estimations, and the velocity dispersion of the clusters. We classified clusters as actual counterparts if they were well aligned with the SZ source, optically rich, and presented high σ_v (Flag = 1). Also, clusters showing high R and good alignment, but with no MOS observations yet available, were classified as potentially confirmed clusters with Flag = 2. Clusters poorly associated with the corresponding SZ source characterized by too-low σ_v or bad alignment were classified with Flag = 3, and non-detections are regions with no galaxy concentration detected. Clusters flagged as "3" and ND make up the unconfirmed cluster sample.

Following this classification, we found 53 confirmed counterparts, which means that 46% of this PSZ1 subsample were validated and characterized using optical data. Sixty-two SZ sources remain unconfirmed. The cluster confirmations include 56 spectroscopic redshift determinations retrieved using long-slit and MOS observations. Table A.1 contains six multiple detections, for which a projection effect of two or more clusters can be associated with the SZ signal. We found two fossil systems, one cluster showing strong lensing effects and several systems with evidence of substructure. New spectroscopic redshifts are supplied for ACO 307, [ATZ98] B100, and ZwCl 0401.8+0219 galaxy clusters.

We found evidence for the effect of galactic dust contamination in the SZ detections. Galactic cirrus is present in the optical images, mainly in regions of low galactic latitude. We found that 61% of SZ sources at low galactic latitudes ($|b| < 25°$) remained unconfirmed; this fraction is a bit lower (47%) for SZ sources at $|b| > 25°$. These numbers suggest that the presence of galactic dust and gas can lead to spurious SZ signals. Moreover, galactic dust contamination (together with other effects, such as Eddington bias and noise inhomogeneities in the *Planck* SZ detections) may distort the SZ S/N estimation. The optical characterization, based on photometric and spectroscopic observations such us the work presented here represents an example of the need to use these kinds of techniques to validate and characterize SZ surveys.

The optical follow-up observations have recently terminated at the ORM, using the facilites described in this paper. We are currently analysing new *Planck* PSZ1 and PSZ2 data, the results of which will be published in the near future.

References

Abell, G. O., Corwin, Jr. H. G., & Olowin, R. P. 1989, ApJS, 70, 1
Aihara, H., Allende Prieto, C., An, D., et al. 2011, ApJS, 193, 29
Allen, S. W., Evrard, A. E., & Mantz, A. B. 2011, ARA&A, 49, 409
Appenzeller, I., Thiering, I., Zickgraf, F.-J., et al. 1998, ApJS, 117, 319
Barrena, R., Girardi, M., Boschin, W., & Mardirossian, F. 2012, A&A, 540, A90
Bertin, E., & Arnouts, S. 1996, A&AS, 117, 393
Bleem, L. E., Stalder, B., de Haan, T., et al. 2015, ApJS, 216, 27
Birkinshaw, M. 1999, Phys. Rep., 310, 97
Böhringer, H., Voges, W., Huchra, J. P., et al. 2000, ApJS, 129, 435
Böhringer, H., Schuecker, P., Guzzo, L., et al. 2001, A&A, 369, 826
Böhringer, H., Chon, G., Collins, C. A., et al. 2013, A&A, 555, A30
Böhringer, H., Chon, G., & Collins, C. A. 2014, A&A, 570, A31
Borgani, S., & Guzzo, L. 2001, Nature, 409, 39
Carlstrom, J. E., Holder, G. P., & Reese, E. D. 2002, ARA&A, 40, 643
Ebeling, H., Edge, A. C., & Henry, J. P. 2001, ApJ, 553, 668
Eddington, A. S. 1913, MNRAS, 73, 359
Gladders, M. D., & Yee, H. K. C. 2000, AJ, 120, 2148
Hao, J., McKay, T. A., Koester, B. P., et al. 2010, ApJS, 191, 254
Hasselfield, M., Hilton, M., Marriage, T. A., et al. 2013, J. Cosmol. Astropart. Phys., 7, 8
Henry, J. P., Evrard, A. E., Hoekstra, H., Babul, A., & Mahdavi, A. 2009, ApJ, 691, 1307
Jones, L. R., Ponman, T. J., Horton, A., et al. 2003, MNRAS, 343, 627
Kennicutt, Jr., R. C. 1992, ApJS, 79, 255
Koester, B. P., McKay, T. A., Annis, J., et al. 2007, ApJ, 660, 239
Komatsu, E., Smith, K. N., Dunkley, J., et al. 2011, ApJS, 192, 18
Liu, J., Hennig, C., Desai, S., et al. 2015, MNRAS, 449, 3370
Magnier, E. A., Schlafly, E., Finkbeiner, D., et al. 2013, ApJS, 205, 20
Mantz, A., Allen, S. W., Rapetti, D., & Ebeling, H. 2010, MNRAS, 406, 1759
Mantz, A. B., von der Linden, A., Allen, S. W., et al. 2015, MNRAS, 446, 2205
Marriage, T. A., Acquaviva, V., Ade, P. A. R., et al. 2011, ApJ, 737, 61
Munari, E., Biviano, A., Borgani, S., Murante, G., & Fabjan, D. 2013, MNRAS, 430, 2638
Planck Collaboration VIII. 2011, A&A, 536, A8
Planck Collaboration IX. 2011, A&A, 536, A9
Planck Collaboration I. 2014, A&A, 571, A1
Planck Collaboration XX. 2014, A&A, 571, A20
Planck Collaboration XXI. 2014, A&A, 571, A21
Planck Collaboration XXIX. 2014, A&A, 571, A29
Planck Collaboration XXXII 2015, A&A, 581, A14
Planck Collaboration XXIV. 2016, A&A, 594, A24
Planck Collaboration XXVII. 2016, A&A, 594, A27
Planck Collaboration Int I. 2012, A&A, 543, A102
Planck Collaboration Int IV. 2013, A&A, 550, A130
Planck Collaboration Int XXVI. 2015, A&A, 582, A29
Planck Collaboration Int XXXVI. 2016, A&A, 586, A139
Pratt, G. W., Pointecouteau, E., Arnaud, M., & Van der Burg, R. F. J. 2016, A&A, 590, L1
Reichardt, C. L., Stalder, B., Bleem, L. E., et al. 2013, ApJ, 763, 127
Rozo, E., Rykoff, E. S., Bartlett, J. G., & Melin, J.-B. 2015, MNRAS, 450, 592
Rykoff, E. S., Rozo, E., Busha, M. T., et al. 2014, ApJ, 785, 104
Springel, V., White, S. D. M., Jenkins, A., et al. 2005, Nature, 435, 629
Staniszewski, Z., 2009, ApJ, 701, 32
Streblyanska, A., Barrena, R., Rubiño-Martín, J. A., et al. 2018, A&A, submitted
Sunyaev, R. A., & Zeldovich, Y. B. 1972, Comments on Astrophysics and Space Physics, 4, 173
Szabo, T., Pierpaoli, E., Dong, F., Pipino, A., & Gunn, J. 2011, ApJ, 736, 21
Tonry, J., & Davis, M. 1979, AJ, 84, 1511
Vanderlinde, K., Crawford, T. M., de Haan, K. A., et al. 2010, ApJ, 722, 1180
van der Burg, R. F. J., Aussel, H., Pratt, G. W., et al. 2016, A&A 587, A23
Vikhlinin, A., Kravtsov, A. V., Burenin, R. A., et al. 2009, ApJ, 692, 1060
Voevodkin, A., Borozdin, K., Heitmann, K., et al. 2010, ApJ, 708, 1376
Voges, W., Aschenbach, B., Boller, T., et al. 1999, A&A, 349, 389
Voges, W., Aschenbach, B., Boller, T., et al. 2000, IAU Circ., 7432, 3
Wen, Z. L., Han, J. L., & Liu, F. S. 2009, ApJS, 183, 197
Wen, Z. L., Han, J. L., & Liu, F. S. 2012, ApJS, 199, 34
Williamson, R., Benson, B. A., Vanderlinde, K., et al. 2011, ApJ, 738, 139
Wright, E. L., Eisenhardt, P. R. M., Mainzer, A. K., et al. 2010, AJ, 140, 1868
Zwicky, F., Herzog, E., Wild, P., Karpowicz, M., & Kowal, C. T. 1961, Catalogue of galaxies and of clusters of galaxies (Pasadena: CIT), 1

Appendix A: Cluster validation catalogue

Table A.1. Clusters candidates from the PSZ1 catalogue studied in this work.

ID[1]	*Planck* Name	SZ S/N	Position (J2000) RA	Position (J2000) Dec	Dist.(')	$\langle z_{spec}\rangle$; $z_{spec,BCG}$	N_{spec}	z_{phot}	R	Flag	Notes
4	PSZ1 G001.00+25.71	6.04	–	–	–	–	–	–	–	ND	
56	PSZ1 G021.88+17.75	5.64	17 28 16.01	−01 22 58.04	2.58	0.646; 0.6488	10	0.60 ± 0.07	44 ± 6.6	1	
67	PSZ1 G027.31+23.79	5.10	–	–	–	–	–	–	–	ND	
68	PSZ1 G027.75+15.41	4.67	–	–	–	–	–	–	–	ND	
69	PSZ1 G027.95+15.63	4.77	–	–	–	–	–	–	–	ND	
70-A	PSZ1 G028.01+25.46	5.98	17 11 54.45	+07 23 13.37	5.16	0.658; 0.6641	9	0.61 ± 0.06	17 ± 4.1	1	Liu+15 report a different counterpart
70-B			17 11 21.53	+07 19 23.17	6.01		–	0.60 ± 0.06	18 ± 4.2	3	
72	PSZ1 G028.15−08.63	5.07	–	–	–	–	–	–	–	ND	
78	PSZ1 G029.79−17.37	6.59	–	–	–	–	–	–	–	ND	
79	PSZ1 G030.21−16.91	5.34	–	–	–	–	–	–	–	ND	
80	PSZ1 G030.70+09.47	4.66	18 13 58.80	+02 22 32.30	4.90	0.052; 0.0532	17	0.11 ± 0.02	62 ± 7.9	1	
82	PSZ1 G030.98+22.43	4.98	17 27 59.37	+08 23 50.10	6.10	0.424; 0.4236	2	0.50 ± 0.06	17 ± 4.1	3	vdB+16 report no counterpart
84	PSZ1 G031.41+28.75	4.84	17 04 58.60	+11 27 01.00	1.27	0.230; 0.2304	4	0.24 ± 0.03	16 ± 4.0	3	
88	PSZ1 G032.15−14.93	8.21	19 43 11.20	−07 24 56.25	4.89	0.377; 0.3775	10	0.43 ± 0.04	51 ± 7.1	3	Substructured
90	PSZ1 G032.76+42.33	4.68	16 15 05.78	+17 46 52.20	0.48	0.844; 0.8431	8	0.67 ± 0.05	39 ± 6.2	1	
91	PSZ1 G033.33−17.54	5.78	19 54 59.67	−07 30 34.70	2.57		–	0.33 ± 0.04	23 ± 4.8	2	
98	PSZ1 G036.02+12.21	4.70	–	–	–	–	–	–	–	ND	
99	PSZ1 G036.09−17.40	5.35	–	–	–	–	–	–	–	ND	
101	PSZ1 G037.22−16.24	5.02	–	–	–	–	–	–	–	ND	
121	PSZ1 G042.96+19.11	4.70	17 58 55.06	+17 13 33.40	2.45	0.499; 0.4993	8	0.53 ± 0.05	45 ± 6.7	1	Substructured
126	PSZ1 G044.82−31.66	4.67	21 04 46.58	−04 45 44.50	2.14	0.221; 0.2213	7	0.21 ± 0.02	23 ± 4.8	3	Liu+15 cluster 126
127	PSZ1 G044.83+10.02	7.27	–	–	–	–	–	–	–	ND	
133	PSZ1 G045.54+16.26	4.67	18 14 13.31	+18 17 03.61	2.18	0.206; 0.2058	21	0.22 ± 0.02	49 ± 7.0	1	
136	PSZ1 G046.02−09.13	4.74	–	–	–	–	–	–	–	ND	
139	PSZ1 G046.35−06.83	4.80	–	–	–	–	–	–	–	ND	
143	PSZ1 G047.44+37.39	4.92	16 50 20.41	+26 58 21.40	3.18	0.230; 0.2318	10	0.23 ± 0.02	17 ± 4.1	1	
144	PSZ1 G047.53+08.55	5.82	–	–	–	–	–	–	–	ND	
158	PSZ1 G050.01−16.88	5.29	–	–	–	–	–	–	–	ND	
163	PSZ1 G052.93+10.44	4.91	18 49 11.97	+22 26 39.36	4.09	0.219; 0.2194	10	0.24 ± 0.03	12 ± 3.5	1	vdB+16 report no counterpart
165	PSZ1 G053.50+09.56	5.11	–	–	–	–	–	–	–	ND	
170	PSZ1 G054.59−18.18	5.33	20 36 38.70	+09 47 53.70	4.40	0.446; 0.4492	4	0.38 ± 0.04	14 ± 3.7	ND	
176[a]	PSZ1 G055.83−41.64	5.72	21 56 41.02	−02 32 20.87	8.29		–	0.63 ± 0.04	16 ± 4.0	3	
179	PSZ1 G056.76−11.60	6.56	20 18 57.20	+15 07 18.3	1.41	0.123; 0.1217	21	–	66 ± 8.1	1	
184	PSZ1 G057.42−10.77	4.76	20 17 25.72	+16 03 27.30	2.10	0.136; 0.1360	25	0.06 ± 0.02	34 ± 5.8	1	
192	PSZ1 G058.45−33.47	4.83	–	–	–	–	–	–	–	ND	
213	PSZ1 G065.13+57.53	4.70	15 16 02.04	+39 44 26.40	2.71	0.684; 0.6857	20	0.69 ± 0.04	78 ± 8.8	1	Substructured
239[a]	PSZ1 G071.64−42.76	8.82	22 30 50.00	+05 39 16.72	1.88		–	0.69 ± 0.08	7 ± 2.6	ND	vdB+16 invalidate this source
251-A	PSZ1 G075.29+26.66	5.17	18 08 44.26	+47 41 09.22	5.85	0.281; 0.2816	10	0.21 ± 0.03	16 ± 4.0	1	
251-B			18 09 09.02	+47 49 01.11	5.98		–	0.25 ± 0.03	17 ± 4.1	2	
257[a]	PSZ1 G078.39+46.13	4.90	16 09 01.45	+50 05 11.32	7.46	0.400; 0.3999	4	0.41 ± 0.04	38 ± 6.2	3	Liu+15 cluster 257
261	PSZ1 G079.88+14.97	4.71	19 23 12.07	+48 16 13.25	0.91	0.101; 0.1020	12	0.07 ± 0.02	56 ± 7.5	1	
271[a]	PSZ1 G081.56+31.03	4.71	17 45 54.62	+53 48 45.96	3.33		–	0.79 ± 0.06	22 ± 4.7	2	vdB+16 invalidate this source
279	PSZ1 G084.04+58.75	4.84	14 49 00.90	+48 33 24.00	2.98	0.735; 0.7302	5	0.70 ± 0.06	58 ± 7.6	1	

Notes. [1] SZ targets identified with the ID followed by an "A", "B" or "C" label indicate the presence of multiple counterparts. [a] Photometric and/or spectroscopic redshift obtained from SDSS DR12 data.

Table A.1. continued.

ID[1]	Planck Name	SZ S/N	RA	Dec	Dist.(')	⟨z_{spec}⟩; $z_{spec,BCG}$	N_{spec}	z_{phot}	R	Flag	Notes
			Position (J2000)								
289	PSZ1 G085.71+10.67	5.35	20 03 13.30	+51 20 51.00	1.56	0.084; 0.0804	12	0.06 ± 0.02	70 ± 8.4	1	Liu+15 report a counterpart at z_{phot} =0.207
305	PSZ1 G090.14−49.71	4.82	–	–	–	–	–	–	–	ND	
306-A	PSZ1 G090.48+46.89	4.90	15 45 18.76	+57 43 37.59	3.82	–	–	0.54 ± 0.04	15 ± 3.9	3	
306-B			15 44 07.40	+57 46 43.20	9.26	0.676; 0.6725	6	0.70 ± 0.05	22 ± 4.7	3	
310[a]	PSZ1 G091.14−38.73	4.79	23 09 10.67	+17 47 38.29	3.19	0.105; 0.1048	1	0.10 ± 0.02	42 ± 6.5	2	
314	PSZ1 G091.93+35.48	5.18	17 09 52.64	+62 22 07.67	2.16	0.276; 0.2755	14	0.26 ± 0.02	30 ± 5.5	3	Liu+15 cluster 314
318	PSZ1 G092.46−35.25	5.47	–	–	–	–	–	–	–	ND	
320	PSZ1 G093.04−32.38	5.69	23 02 15.07	+24 03 50.50	7.48	0.512; 0.5104	5	0.55 ± 0.05	42 ± 6.5	3	
331	PSZ1 G094.95−36.72	4.79	23 16 25.10	+20 57 23.90	1.79	–	–	0.50 ± 0.05	19 ± 4.4	2	
336	PSZ1 G096.44−10.40	6.55	22 20 12.95	+44 26 16.27	8.17	0.195; 0.1948	4	0.22 ± 0.03	14 ± 3.7	ND	
348	PSZ1 G098.67−07.03	4.99	–	–	–	–	–	–	–	ND	
349	PSZ1 G098.85−07.27	4.87	–	–	–	–	–	–	–	ND	
356	PSZ1 G099.63+14.85	4.72	–	–	–	–	–	–	–	ND	
361[a]	PSZ1 G100.46−61.45	4.71	00 09 15.84	−00 26 58.94	1.61	0.256; 0.2561	1	0.28 ± 0.02	18 ± 4.2	2	
369	PSZ1 G102.97−04.77	5.64	22 34 47.08	+52 42 55.56	0.31	–	–	0.52 ± 0.04	27 ± 5.2	2	
370	PSZ1 G103.16−14.95	5.08	23 04 00.34	+43 46 21.40	1.99	–	–	0.27 ± 0.03	13 ± 3.6	ND	
375	PSZ1 G103.94+25.81	4.78	18 52 09.50	+72 59 33.12	1.96	0.077; 0.0777	17	0.06 ± 0.02	66 ± 8.1	1	Liu cluster 375. Fossil system
377	PSZ1 G104.78+40.45	4.92	15 46 29.88	+69 57 59.11	2.16	0.837; 0.8373	10	0.70 ± 0.06	40 ± 6.3	1	
382	PSZ1 G106.07−17.42	4.73	23 23 20.46	+42 33 15.32	1.89	0.817; 0.8144	10	0.65 ± 0.07	21 ± 4.6	3	
385	PSZ1 G106.49−10.43	5.40	23 10 58.60	+49 12 28.21	3.80	–	–	0.49 ± 0.05	9 ± 3.0	ND	
387	PSZ1 G106.81−36.44	4.66	–	–	–	–	–	–	–	ND	
393	PSZ1 G108.13−09.21	5.39	–	–	–	–	–	–	–	ND	
395	PSZ1 G108.26+48.66	4.88	14 27 04.57	+65 39 46.94	1.06	0.671; 0.6752	29	0.69 ± 0.06	34 ± 5.8	1	Substructured
397	PSZ1 G108.90−52.04	6.89	00 16 26.74	+09 53 53.60	2.88	0.461; 0.4620	4	0.54 ± 0.04	23 ± 4.8	2	
412	PSZ1 G112.60−39.30	4.76	–	–	–	–	–	–	–	ND	
420	PSZ1 G114.81−11.80	4.85	00 01 14.70	+50 16 32.16	2.48	0.228; 0.2281	1	0.21 ± 0.02	38 ± 6.2	2	Inlcuded in RTT150 work
421	PSZ1 G114.98+19.10	5.19	–	–	–	–	–	–	–	ND	
436	PSZ1 G118.61+10.55	4.96	23 53 24.56	+72 59 00.33	3.11	–	–	0.77 ± 0.07	50 ± 7.1	2	
444	PSZ1 G121.27+23.08	4.72	–	–	–	–	–	–	–	ND	
446	PSZ1 G121.69+24.47	5.35	–	–	–	–	–	–	–	ND	
449	PSZ1 G123.37+25.34	5.90	01 45 31.18	+88 12 16.91	2.48	–	–	0.95 ± 0.11	22 ± 4.7	2	
453	PSZ1 G123.79+25.86	5.04	03 00 48.59	+88 30 09.18	1.31	–	–	0.54 ± 0.04	48 ± 6.9	2	
456	PSZ1 G124.64+29.38	4.89	10 35 55.45	+87 16 34.35	1.39	–	–	0.35 ± 0.03	36 ± 6.0	2	
458-A[a]	PSZ1 G125.54−56.25	4.86	00 57 09.25	+06 35 05.92	2.04	0.548; 0.5475	1	0.59 ± 0.04	26 ± 5.1	2	
458-B[a]			00 57 08.83	+06 34 06.14	2.49	0.168; 0.1676	1	0.17 ± 0.02	32 ± 5.7	2	
458-C[a]			00 57 22.23	+06 38 27.27	3.29	0.296; 0.2961	1	0.27 ± 0.03	33 ± 5.7	2	
462[a]	PSZ1 G126.44−70.36		00 55 57.36	−07 33 42.46	4.20	0.325; 0.3246	3	0.33 ± 0.04	21 ± 4.6	2	
465	PSZ1 G127.36−10.69	5.58	–	–	–	–	–	–	–	ND	
468	PSZ1 G128.75−17.97	4.95	–	–	–	–	–	–	–	ND	
476	PSZ1 G133.50−46.77	4.91	01 21 25.03	+15 30 56.84	1.38	–	–	0.68 ± 0.09	14 ± 3.7	ND	
478	PSZ1 G134.08−44.61	5.42	–	–	–	–	–	–	–	ND	
479	PSZ1 G134.31−06.57	4.81	02 10 25.10	+54 34 09.80	1.61	0.333; 0.3341	20	0.35 ± 0.03	64 ± 8.0	1	
490	PSZ1 G135.92+76.21	5.22	12 35 46.89	+40 27 55.53	6.29	0.406; –	9	0.39 ± 0.04	14 ± 3.7	ND	
492	PSZ1 G136.37−44.50	4.90	–	–	–	–	–	–	–	ND	
496	PSZ1 G137.51−10.01	5.33	02 22 53.51	+50 14 40.11	1.93	–	–	0.14 ± 0.02	67 ± 8.2	2	
497	PSZ1 G137.56+53.88	5.73	–	–	–	–	–	–	–	ND	
504	PSZ1 G140.10+50.09	4.90	11 11 30.47	+63 35 16.76	5.33	–	–	0.70 ± 0.05	26 ± 5.1	3	

Table A.1. continued.

ID[1]	*Planck* Name	SZ S/N	Position (J2000) RA	Position (J2000) Dec	Dist.(')	⟨z_{spec}⟩; $z_{spec,BCG}$	N_{spec}	z_{phot}	R	Flag	Notes
509	PSZ1 G142.17+37.28	579	09 19 05.16	+70 55 11.40	3.26	0.240; 0.2393	6	0.23 ± 0.03	74 ± 8.6	1	Liu+15 report a z_{phot} = 0.28
511	PSZ1 G142.38+22.82	5.81	06 13 49.84	+71 52 54.78	0.96	0.394; 0.3927	2	0.34 ± 0.05	20 ± 4.5	2	
529	PSZ1 G148.20+23.49	8.40	06 37 54.60	+66 51 06.20	3.42	0.098; 0.0980	2	–	35 ± 5.9	2	Liu+15 cluster 529
534	PSZ1 G150.33−20.04	4.75	02 59 31.65	+35 56 30.47	11.7	–	–	0.07 ± 0.01	15 ± 3.9	ND	
539	PSZ1 G151.80−48.06	5.59	02 08 07.55	+10 27 17.54	0.98	0.201; 0.1999	2	–	23 ± 4.8	2	ACO 307
549	PSZ1 G157.07−33.66	4.90	02 51 35.96	+21 07 05.30	0.60	–	–	0.62 ± 0.05	21 ± 4.6	2	vdB+16 invalidate this source
551	PSZ1 G157.44+30.34	7.54	07 48 54.35	+59 42 05.77	1.46	0.407; 0.4046	4	0.34 ± 0.03	18 ± 4.2	2	[ATZ98] B100
564	PSZ1 G162.30−26.92	6.56	03 24 19.02	+23 57 49.82	3.37	0.391; 0.3917	3	0.73 ± 0.07	44 ± 6.6	2	
586-A	PSZ1 G169.80+26.10	5.32	07 30 32.02	+48 17 39.05	4.21	–	–	0.83 ± 0.10	36 ± 6.0	2	
586-B			07 30 29.09	+48 20 39.15	3.53	–	–	0.38 ± 0.03	19 ± 4.6	ND	
605	PSZ1 G178.10+18.58	5.01	07 01 31.33	+38 52 48.60	9.28	–	–	0.41 ± 0.04	12 ± 3.5	2	
612	PSZ1 G181.21−30.73	5.87	04 02 56.76	+09 44 29.10	0.76	0.540; 0.5406	3	0.62 ± 0.05	26 ± 5.1	2	Liu+15 cluster 612
618-A	PSZ1 G183.26+12.25	5.43	06 43 09.84	+31 50 55.47	3.44	0.638; 0.6352	2	0.27 ± 0.03	25 ± 5.0	2	See Fig. 2
618-B			06 42 58.24	+31 45 01.07	4.12	–	–	0.08 ± 0.02	23 ± 4.8	2	
624	PSZ1 G185.42−32.03	6.15	04 07 50.12	+06 07 06.29	1.76	–	–	0.11 ± 0.02	43 ± 6.6	2	
626	PSZ1 G185.93−31.21	5.90	04 11 52.31	+06 17 11.80	3.47	0.094; 0.0947	2	–	22 ± 4.7	2	Fossil system
634	PSZ1 G188.36−35.00	5.28	04 04 18.02	+02 23 55.46	1.30	0.275; 0.2723	4	–	29 ± 5.4	1	ZwCl 0401.8+0219
641	PSZ1 G189.82−37.25	6.99	–	–	–	–	–	0.75 ± 0.10	–	ND	
653	PSZ1 G194.74−10.10	5.19	05 41 05.73	+11 10 05.32	0.76	–	–	0.75 ± 0.10	30 ± 5.5	2	
653	PSZ1 G194.74−10.10	5.19	05 41 05.73	+11 10 05.32	0.76	–	–	0.44 ± 0.04	30 ± 5.5	2	
682	PSZ1 G206.45+13.89	5.90	07 29 51.23	+11 56 30.89	1.97	0.406; 0.4055	45	–	127 ± 11.2	1	Gravitational arc
684	PSZ1 G206.64−21.17	6.62	–	–	–	–	–	0.15 ± 0.02	–	ND	
713	PSZ1 G216.27+10.10	5.16	07 33 20.03	+01 36 36.06	3.14	–	–	0.24 ± 0.03	31 ± 5.6	2	
723	PSZ1 G218.54+13.26	5.24	07 48 51.66	+01 06 39.88	1.80	0.266; 0.2682	16	0.25 ± 0.03	77 ± 8.8	1	
752	PSZ1 G224.82+13.62	5.51	08 01 41.61	−04 03 46.23	0.14	0.274; 0.2759	28	0.15 ± 0.02	132 ± 11.5	1	
827	PSZ1 G244.48+34.06	8.14	09 49 46.96	−07 30 12.50	1.40	0.135; 0.1342	7	0.18 ± 0.03	23 ± 4.8	3	
992	PSZ1 G286.25+62.68	5.52	12 21 05.35	+00 48 22.29	1.46	0.211; 0.2107	11	–	48 ± 6.9	3	
1122	PSZ1 G318.61+83.80	6.93	–	–	–	–	–	0.06±0.02	–	ND	
1159[a]	PSZ1 G332.30+72.17	4.76	13 26 33.96	+11 18 06.51	2.96	0.089; 0.0898	30	0.25±0.03	64 ± 8.0	1	Liu+15 cluster 1159
1189	PSZ1 G341.69+50.66	5.48	14 25 12.29	−04 56 34.19	3.90	0.293; 0.2913	31	–	35 ± 5.9	1	Substructured. Liu+15 cluster
1198	PSZ1 G345.81+42.38	4.80	–	–	–	–	–	–	–	ND	
1212	PSZ1 G352.04+42.25	4.74	–	–	–	–	–	0.13±0.02	–	ND	
1221	PSZ1 G357.43+30.60	5.47	15 54 53.89	−12 13 16.75	4.45	–	–		13±3.6	ND	